

Cargo- and adaptor-specific mechanisms regulate clathrin-mediated endocytosis

Marcel Mettlen,¹ Dinah Loerke,² Defne Yazar,¹ Gaudenz Danuser,¹ and Sandra L. Schmid¹

¹Department of Cell Biology, The Scripps Research Institute, La Jolla, CA 92037

²Department of Physics and Astronomy, University of Denver, Denver, CO 80208

Clathrin-mediated endocytosis of surface receptors and their bound ligands (i.e., cargo) is highly regulated, including by the cargo itself. One of the possible sources of the observed heterogeneous dynamics of clathrin-coated pits (CCPs) might be the different cargo content. Consistent with this, we show that CCP size and dynamic behavior varies with low density lipoprotein receptor (LDLR) expression levels in a manner dependent on the LDLR-specific adaptors, Dab2 and ARH. In Dab2-mCherry-expressing cells, varying LDLR expression

leads to a progressive increase in CCP size and to the appearance of nonterminal endocytic events. In LDLR and ARH-mCherry-expressing cells in addition to an increase in CCP size, turnover of abortive CCPs increases, and the rate of CCP maturation decreases. Altogether, our results underscore the highly dynamic and cargo-responsive nature of CCP assembly and suggest that the observed heterogeneity is, in part, related to compositional differences (e.g., cargo and adaptors) between CCPs.

Introduction

Clathrin-mediated endocytosis (CME) requires the coordination of multiple molecular events for the assembly and maturation of clathrin-coated pits (CCPs), including incorporation of transmembrane receptors (hereafter referred to as cargo) through selective adaptor proteins. Recently, based on lifetime decomposition, we identified three CCP subpopulations, termed early abortive, late abortive, and productive CCPs (Loerke et al., 2009). Our data suggested that aberrant structures not suited for completion abort, whereas productive CCPs are stabilized and complete their maturation to form endocytic clathrin-coated vesicles (CCVs). Thus, the overall rate of CME measured biochemically depends on four variables: the (i) density/number of productive CCPs, (ii) efficiency of CCP maturation, (iii) rate of CCP maturation, and (iv) cargo/CCP, which in turn depends on CCP size and/or the packaging efficiency of cargo molecules. Our data also suggested the existence of an endocytic restriction/

checkpoint mechanism that receives input through endocytic accessory proteins, monitoring among other factors coat assembly, membrane curvature, and cargo selection (Loerke et al., 2009; Mettlen et al., 2009). The incorporation of certain cargo/adaptor protein complexes (i.e., transferrin receptor/AP2) into CCPs increases the efficiency of CCP maturation without affecting CCP density or CCP maturation rate (Loerke et al., 2009; Mettlen et al., 2009). Whether other cargo, using other adaptor proteins, have the same effect, is yet unknown.

Transferrin (Tfn) and low density lipoprotein (LDL) receptors (TfnRs and LDLRs, respectively) are concentrated in CCPs and constitutively endocytosed even in the absence of their nutrient ligands (Hanover et al., 1985; Brodsky, 1988). The clustering of these cargos depends on sorting signals found in their cytoplasmic tail (Trowbridge et al., 1993; Kirchhausen et al., 1997). Whereas the YXXΦ sorting signal in the TfnR (Jing et al., 1990) is recognized by the tetrameric adaptor protein AP2, recruitment of the LDLR relies on an FXNPXY motif (Davis et al., 1986) recognized by the adaptors Dab2 and ARH. Interestingly, although LDLR uptake in cultured hepatocytes and lymphocytes is dependent on ARH (Mishra et al., 2002b; Jones et al., 2003),

Correspondence to Sandra L. Schmid: slschmid@scripps.edu

D. Yazar's present address is Whitehead Institute, Massachusetts Institute of Technology, 9 Cambridge Ctr., Cambridge, MA 02142.

G. Danuser's present address is Department of Cell Biology, 240 Longwood Ave., Harvard Medical School, Boston, MA 02115.

Abbreviations used in this paper: CCP, clathrin-coated pit; CCS, clathrin-coated structure; CCV, clathrin-coated vesicle; CME, clathrin-mediated endocytosis; EGFP, enhanced GFP; GCCS, giant CCS; LCa, light chain α; LDLR, low density lipoprotein receptor; tet, tetracycline; TfnR, transferrin receptor; TIR-FM, total internal reflection fluorescence microscopy; wt, wild type.

© 2010 Mettlen et al. This article is distributed under the terms of an Attribution–Noncommercial–Share Alike–No Mirror Sites license for the first six months after the publication date [see <http://www.rupress.org/terms>]. After six months it is available under a Creative Commons License (Attribution–Noncommercial–Share Alike 3.0 Unported license, as described at <http://creativecommons.org/licenses/by-nc-sa/3.0/>).

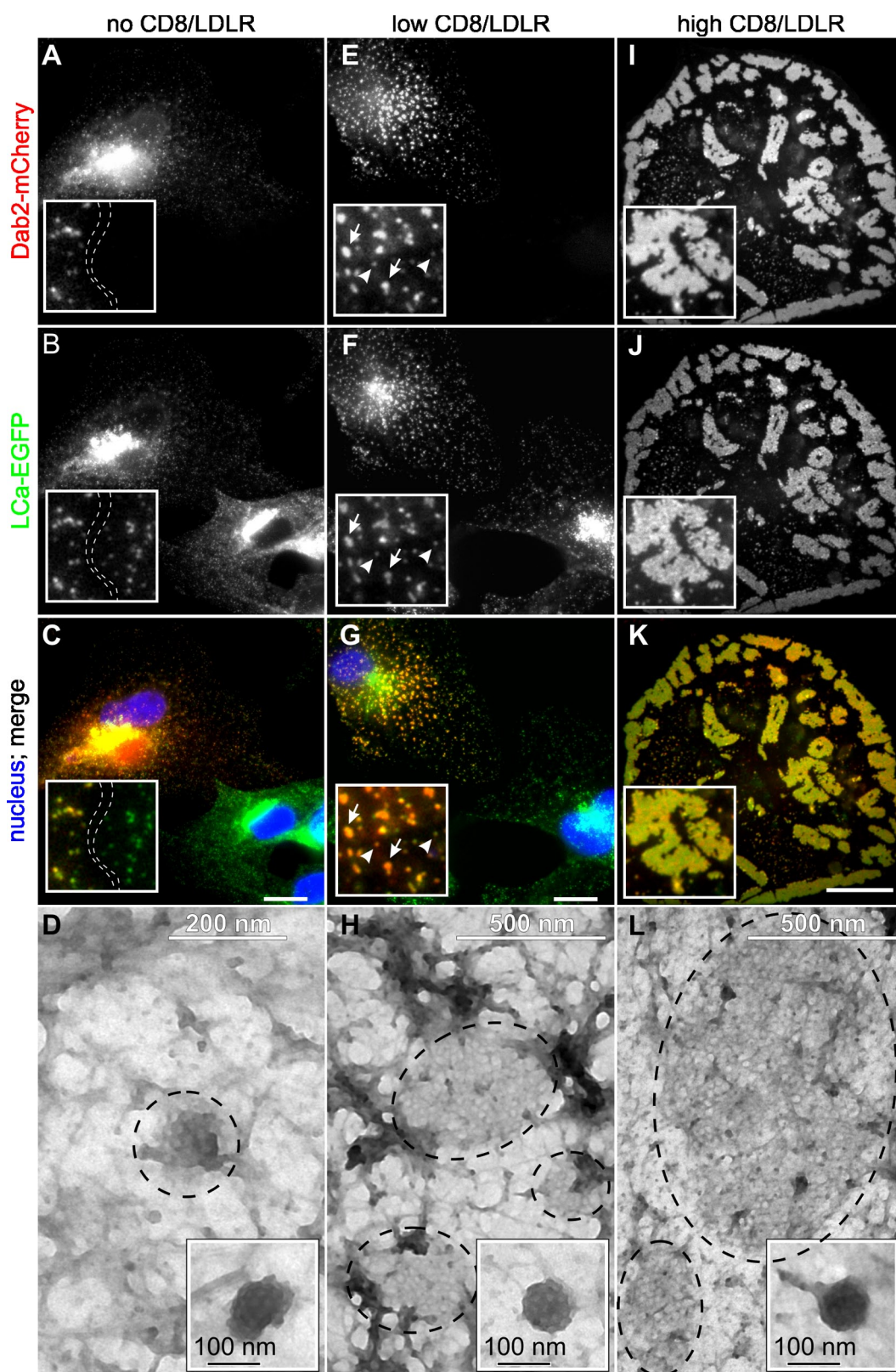


Figure 1. **Dab2/LDLRs regulate CCP size.** BSC1 cells stably expressing LCa-EGFP were transfected with Dab2-mCherry and infected with adenoviruses coding for a tet-repressible LDLR expression system. Cells were cultured in the presence of decreasing concentrations of tet, fixed/permeabilized, and observed by epifluorescence or electron microscopy. [tet]: (A–D) 1,000 ng/ml, no CD8/LDLR; (E–H) 25 ng/ml, low CD8/LDLR; arrowheads: normal-sized CCPs; arrows: enlarged CCPs (I–L): 0 ng/ml, high CD8/LDLR. Bars, 10 μ m. (D, H, and I) Encircled areas indicate clathrin lattices at the ventral membrane of BSC-1 cells. Insets show normal-sized CCPs in each condition.

Table 1. CCP size, as determined by negative-stain EM, varies with cargo, Dab2, and ARH expression levels

Adenovirus construct	Tet (ng/ml)	Adaptor protein expressed	CCP size ($\mu\text{m}^2 \pm \text{SD}$)	n
Ventral cell surface				
CD8/LDLR	1,000	Dab2	0.013 ± 0.03	20
CD8/LDLR	25	Dab2	0.45 ± 0.38^a	19
CD8/LDLR	0	Dab2	3.31 ± 2.49^b	8
CD8/LDLR	0	ARH	0.89 ± 0.54^c	27
Dorsal cell surface				
TfnR	1,000	None	0.011 ± 0.004	51
TfnR	0	None	0.008 ± 0.003^d	82

^aP < 0.001 relative to no CD8/LDLR expression (i.e. 1,000 ng/ml tet).

^bP < 0.001 relative to low levels of CD8/LDLR expression (i.e. 25 ng/ml tet).

^cP < 0.001 relative to Dab2 expression in the presence of high CD8/LDLR levels.

^dP < 0.001 relative to endogenous levels of TfnR expression (i.e. 1,000 ng/ml tet).

its uptake in ARH-null fibroblasts is unaffected (Garcia et al., 2001; Arca et al., 2002). In these cells, Dab2 mediates LDLR internalization, suggesting that these adaptors are partially redundant (Maurer and Cooper, 2006).

Dab2 and ARH both contain N-terminal PTB domains that bind to FXNPXY sorting signals and phosphatidylinositol-4,5-bisphosphate. Dab2, but not ARH, contains multiple NPF motifs that mediate binding of Eps15 homology (EH) domain-containing proteins; whereas a PDZ-interacting motif is present in ARH, but not Dab2. Additional recognition motifs in these adaptors mediate binding to both clathrin and AP2 (Mishra et al., 2002a,b). Although Dab2 interacts with AP2 selectively through the α -adaptin subunit (Morris and Cooper, 2001), it appears to sort cargo into CCPs independently of AP2 (Garuti et al., 2005; Keyel et al., 2006; Maurer and Cooper, 2006). ARH binds selectively to the β -adaptin subunit of AP2 (Mishra et al., 2005; Edeling et al., 2006; Keyel et al., 2008) and its function is AP2 dependent (Maurer and Cooper, 2006). Although the general endocytic functions of ARH and Dab2 have been well established, the relationship between these adaptors and AP2 complexes remains unclear, and there are conflicting reports as to whether LDLR and TfnR are internalized via the same or distinct CCPs (Keyel et al., 2006; Lakadamyali et al., 2006).

Here, we have used BSC1 cells expressing variable levels of a CD8/LDLR chimera along with wild-type (wt) and mutant forms of its adaptors, Dab2 and ARH. Combining total internal reflection fluorescence microscopy (TIR-FM), electron microscopy (EM), and biochemical assays, we have studied the effects of this cargo and its adaptors on the size and dynamic behavior of CCPs and the rate and efficiency of CCP maturation.

Results

To study the effect of LDLR and its specific adaptors on clathrin-mediated endocytosis we used epithelial BSC1 cells because (i) they are well suited for TIR-FM due to their morphology and adherence to the substratum, (ii) they can be readily infected with adenovirus for regulated protein expression, (iii) they contain low

levels of endogenous LDLRs, Dab2 and ARH (Keyel et al., 2006; unpublished data) facilitating analysis of exogenously expressed wild-type and mutant forms of these proteins, and (iv) CCP dynamics in these cells are well characterized (Ehrlich et al., 2004; Loerke et al., 2009; Mettlen et al., 2009). We first examined Dab2, which mediates LDLR uptake independently of AP2.

Relative amounts of Dab2 and CD8/LDLR control CCP size

Stable Dab2 expression strongly inhibits proliferation of cultured cell lines (He et al., 2003; unpublished data); therefore, we transiently transfected BSC1 cells with mCherry-tagged Dab2 (Dab2-mCherry). Under these conditions, Dab2-mCherry colocalized with enhanced GFP (EGFP)-tagged clathrin light chain a (LCa-EGFP; Fig. 1, A–C) and EGFP-tagged σ 2 subunit of AP2 (σ 2-EGFP; Fig. S2 A) in CCPs at the cell surface. This expected localization of Dab2-mCherry suggests that the fluorescent tag did not interfere with its function.

CCPs in Dab2-mCherry-expressing cells were comparable in intensity to those in neighboring cells not expressing Dab2 (Fig. 1 B, inset). Negative-stained EM analysis of CCPs on the exposed ventral surface of cells (Fig. 1 D) revealed small flat and curved lattices, typically <200 nm in diameter (Table I). These results differ from observations made upon Dab2 overexpression in Cos7 and HeLa cells (Chetrit et al., 2009), leading us to hypothesize that these differences might reflect the low endogenous levels of LDLRs (or other Dab2-specific cargo) expressed in BSC1 cells relative to other cell lines (Keyel et al., 2006). To test this hypothesis, we generated recombinant adenoviruses encoding a CD8/LDLR chimera driven by a tetracycline (tet)-repressible promoter. The CD8/LDLR chimera comprises the extracellular and transmembrane domains of CD8 and the intracellular LDLR tail bearing a FXNPXY motif (Motley et al., 2003). In infected BSC1 cells, the expression levels of this chimera can be tightly controlled by tet (Fig. S1, A and B) and its endocytosis readily measured using commercially available anti-CD8 antibodies as ligand.

As predicted, at the low levels of CD8/LDLR expression induced in the presence of 25 ng/ml tet (Fig. S1), CCPs increased in intensity (Fig. 1, E–G), suggesting an increase in CCP size and/or clustering of CCPs. EM analysis of the ventral surface of cells revealed the appearance of larger flat lattices (Fig. 1 H), up to 500 nm in diameter (Table I), and clusters of CCPs (Fig. 1, F and H; see also Fig. 3 Ba) that were not detected under control conditions. Strikingly, at the high levels of overexpression achieved upon complete removal of tet, Dab2 was strongly recruited to the plasma membrane and induced the formation of giant clathrin-coated structures (GCCSs). These were selectively located on the ventral surface, irregular in shape, and reached several micrometers in diameter (Fig. 1, I–L, Fig. S2 B, and Video 1). EM revealed these to be flat lattices (Table I) and not clusters of CCPs. GCCS formation was dependent on Dab2 expression, as they were not detected in cells overexpressing CD8/LDLR alone (Fig. S2, E and F; see also Fig. 4, C and D). When TfnRs were overexpressed, even in the presence of Dab2 (Fig. S2 C), we did not detect an effect on CCP size or the appearance of GCCSs by immunofluorescence. Indeed, in our studies, CCPs detected by EM on the dorsal surface of BSC1 cells overexpressing TfnR

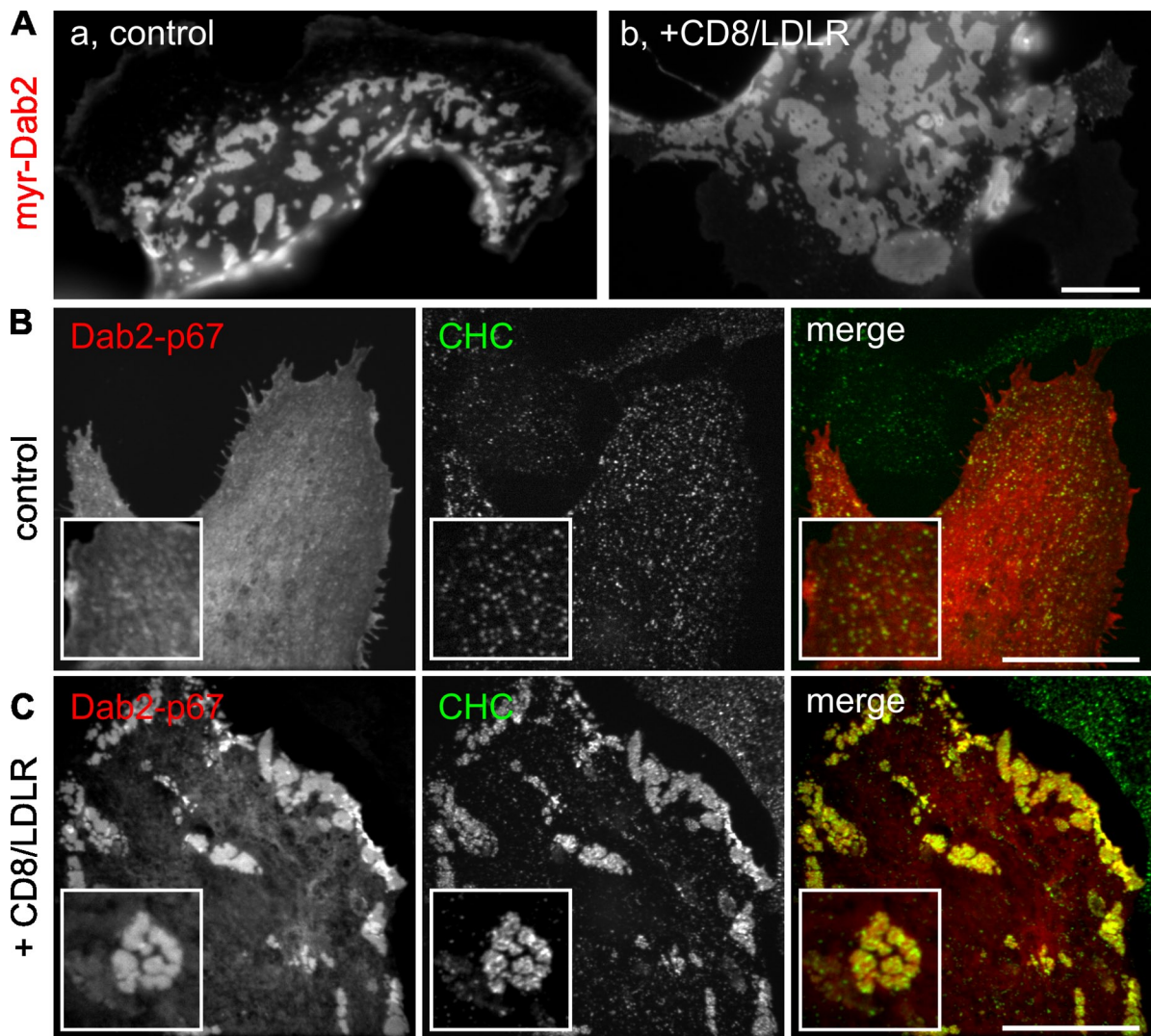


Figure 2. Requirements for Dab2/LDLR-induced GCCS formation. BSC1-wt cells were transfected with either myristoylated Dab2-mCherry (A) or Dab2-p67-mCherry (B and C) and were infected with adenoviruses coding for CD8/LDLR as indicated. Cells were fixed, permeabilized, immunolabeled in green for clathrin heavy chain (CHC; B and C), and observed by epifluorescence. Bars, 10 μ m.

alone were smaller than in control cells (Table I). These findings differ from an earlier study in which the assembly of flat clathrin lattices was induced by overexpression of human TfnR in chicken fibroblasts (Miller et al., 1991), which may reflect species or cell type differences. Together, these results demonstrate a continuum in the size of CCPs dependent on the expression levels of Dab2 and cargo: both Dab2 and CD8/LDLR overexpression are required for the formation of GCCSs.

Increased membrane recruitment of Dab2 is sufficient to induce GCCSs

To test whether direct cargo binding by Dab2 is required for formation of GCCSs, we expressed myristoylated Dab2 in BSC1 cells. Even in the absence of exogenously expressed cargo, the strong membrane recruitment of this protein alone was sufficient to induce GCCSs (Fig. 2 Aa), although CD8/LDLR expression further increased their size (Fig. 2 Ab). Under these conditions, formation of GCCSs was no longer restricted to the ventral plasma membrane (not depicted).

Dab2 exists as two isoforms: Dab2-p96 and the internal splice variant, Dab2-p67 (Xu et al., 1995). Dab2-p96 binds to both clathrin and AP2, and localizes to CCPs, whereas Dab2-p67 lacks the main AP2- and clathrin-binding motifs and does not localize to CCPs. To probe the structural requirements for the formation of Dab2-dependent GCCSs, we expressed mCherry-labeled Dab2-p67 in BSC1 cells and confirmed that under control conditions (Fig. 2 B) and upon overexpression of the TfnR (Fig. S2 D), Dab2-p67 exhibited a mainly diffuse, probably cytosolic labeling with only minor/no recruitment to CCPs. Unexpectedly, in cells overexpressing CD8/LDLR, Dab2-p67 induced the formation of GCCSs and colocalized with clathrin heavy chain (CHC; Fig. 2 C). These observations suggest that in the presence of low levels of cargo, clathrin and/or AP2 binding by Dab2 are required for its recruitment to CCPs. However, at higher cargo concentrations, other binding interactions, perhaps involving the remaining NPF motifs on Dab2-p67, are sufficient to stabilize Dab2 at the membrane, leading to the formation of larger CCPs and ultimately GCCSs.

Dab2 and CD8/LDLR expression can induce clathrin-coated structures (CCSs) that mimic nonterminal endocytic events

To probe the endocytic activity of CCSs in the presence of Dab2 and increasing amounts of CD8/LDLRs, we next observed BSC1 cells by time-lapse TIR-FM. In the absence of CD8/LDLR, Dab2-mCherry and LCa-EGFP displayed typical dynamic behaviors, assembling as CCPs and departing together as CCVs (Fig. 3 A, [Video 2](#)). However, we were also able to detect a small fraction of “nonterminal” events (Fig. 3 A, arrowhead at 140 s), which were originally defined by Merrifield et al. (2005) as sites at which multiple rounds of CCV formation were observed to occur from an apparently single CCP. Nonterminal events are frequently observed in HeLa cells (Merrifield et al., 2005; Loerke et al., 2009), but rarely detected in control BSC1 cells (Ehrlich et al., 2004; Loerke et al., 2009). Our ability to detect nonterminal endocytic events in BSC1 cells expressing Dab2 suggests the existence of some larger-than-normal CCPs or unresolvable clusters of CCPs, even in the presence of endogenous cargo levels.

The larger CCPs present in BSC1 cells expressing Dab2-mCherry and low levels of CD8/LDLR (Fig. 1, E–H) were highly dynamic and often appeared as clusters of smaller CCSs. Indeed, clusters of CCPs were frequently observed by EM (Fig. 3 Ba). Multiple rounds of vesicle budding (Fig. 3 Bb and [Video 3](#)) could be detected from these CCP clusters, which would appear as nonterminal events for closely adjacent CCPs. With increasing amounts of CD8/LDLR, the size of these clusters increased (not depicted), and although Dab2-mCherry was homogeneously distributed throughout these structures, LCa-EGFP and CHC were less uniform (Fig. 1 J and Fig. 3 C). This uneven distribution was even more pronounced for AP2, which appeared as mobile clusters within enlarged CCSs (Fig. S2 B and [Video 4](#)). Finally, GCCSs induced by overexpression of CD8/LDLR and Dab2 also displayed a dynamic morphology (Fig. 3 C, splitting and merging events within these structures are indicated by arrows and arrowheads, respectively; see also [Video 5](#)). Dab2 and clathrin exchanged actively in these structures (Fig. 3 D), albeit with different kinetics (Fig. 3 E; Chetrit et al., 2009). However, despite this dynamic behavior, CCVs were observed to pinch off from the edges of these GCCSs only on rare occasions, indicating that they are not endocytically active (Videos 4 and 5). Together, these data further support a continuum of effects of cargo and Dab2 on CCP size and dynamic behavior.

CCP localization of ARH is cargo dependent

In contrast to Dab2, exogenous expression of ARH did not inhibit cell proliferation, and thus we could generate BSC1 cells stably expressing mCherry-tagged ARH (ARH-mCherry). To our surprise, unlike the identically labeled Dab2, the vast majority of ARH-mCherry was found in the nucleus of BSC1 cells (Fig. 3, A and B). Only a weak ARH signal was detectable in CCPs, colocalizing with CHC (not depicted) and α -adaptin (Fig. 4 B, insets upon overexposure).

Upon CD8/LDLR expression, ARH exited the nucleus and was recruited to the plasma membrane, where it colocalized with clathrin (Fig. 4 C), and α -adaptin (Fig. 4 D) in diffraction-limited

CCPs. Unlike Dab2, the combined presence of ARH and CD8/LDLR did not induce formation of GCCSs. EM analysis showed that the CCPs present in these cells consisted of flat and curved lattices, which remained below the diffraction limit (up to 500-nm and 165-nm diameter, respectively; [Fig. S4 D](#), Table I). When we coexpressed CD8/LDLR, Dab2-mCherry, and ARH-EGFP in BSC1 cells, both adaptors were recruited to the plasma membrane, where they colocalized (Fig. 4 E). However, in the presence of ARH, Dab2 and CD8/LDLR overexpression failed to generate GCCSs, although CCSs remained larger (and/or more clustered) when compared with control conditions (compare Fig. 4 E with Fig. 1, I–K and Fig. 4, C and D). Together, these results indicate that (i) Dab2 and ARH bind to the same cargo, (ii) both adaptors are recruited into the same CCSs, (iii) the size of CCPs can be controlled by the ratio of Dab2/ARH; and (iv) despite their partial functional redundancies and structural similarities, Dab2 and ARH exhibit fundamentally different, albeit cargo-dependent, interactions with CCPs.

We also noted that stable ARH expression altered cell morphology such that the cells displayed a very broad and regular leading edge (Fig. 4 A, [Fig. S3 A](#)). These shape changes were accompanied by alterations in the actin cytoskeleton (Fig. S3, A and B), which were reversed upon CD8/LDLR expression, as ARH redistributed to CCPs (Fig. S3 C). Together, these observations indicate that ARH interacts with and controls actin dynamics by an as yet unknown mechanism.

AP2 binding is required for CCP recruitment of ARH, whereas its nuclear export is passive and AP2 independent

We next examined the structural requirements for the cargo-dependent redistribution of ARH from the nucleus. The mutant mCherry-tagged ARH-F259A, which is unable to bind AP2 (Mishra et al., 2005), was also localized to the nucleus in stably transformed BSC1 cells not expressing CD8/LDLR (Fig. 5 A). Upon overexpression of CD8/LDLR, ARH-F259A exited the nucleus, but was not recruited into CCPs (Fig. 5 B). Thus, although cargo overexpression is sufficient to trigger nuclear exit, AP2 interactions are required to stabilize ARH in CCPs. Consistent with this, ARH-containing CCPs almost always colocalized with AP2 (Fig. 4 D), even though we could readily detect clathrin-labeled CCPs that did not contain AP2 (Fig. S2 E, circles). We next tested the role of ARH's PTB domain in nuclear exit. The PTB domain mutants ARH-S117Y and ARH-F165A show no or reduced affinity for LDLRs, respectively, and fail to rescue LDL-plasma concentrations in ARH^{-/-} mice (Garuti et al., 2005). When transiently transfected into BSC1 cells both the ARH-S117Y-mCherry and ARH-F165A-mCherry mutants exhibited attenuated nuclear exit/CCP recruitment upon CD8/LDLR expression (unpublished data). The double mutant ARH-S117Y;F165A-mCherry was localized to the nucleus and failed to exit upon CD8/LDLR expression (Fig. 5 C), indicating a role for PTB binding interactions in the nuclear shuttling of ARH.

Proteins or protein complexes with a molecular weight larger than ~40 kD are actively transported through nuclear pore complexes by importins. These transporters recognize nuclear localization signals (NLSs) found in target proteins

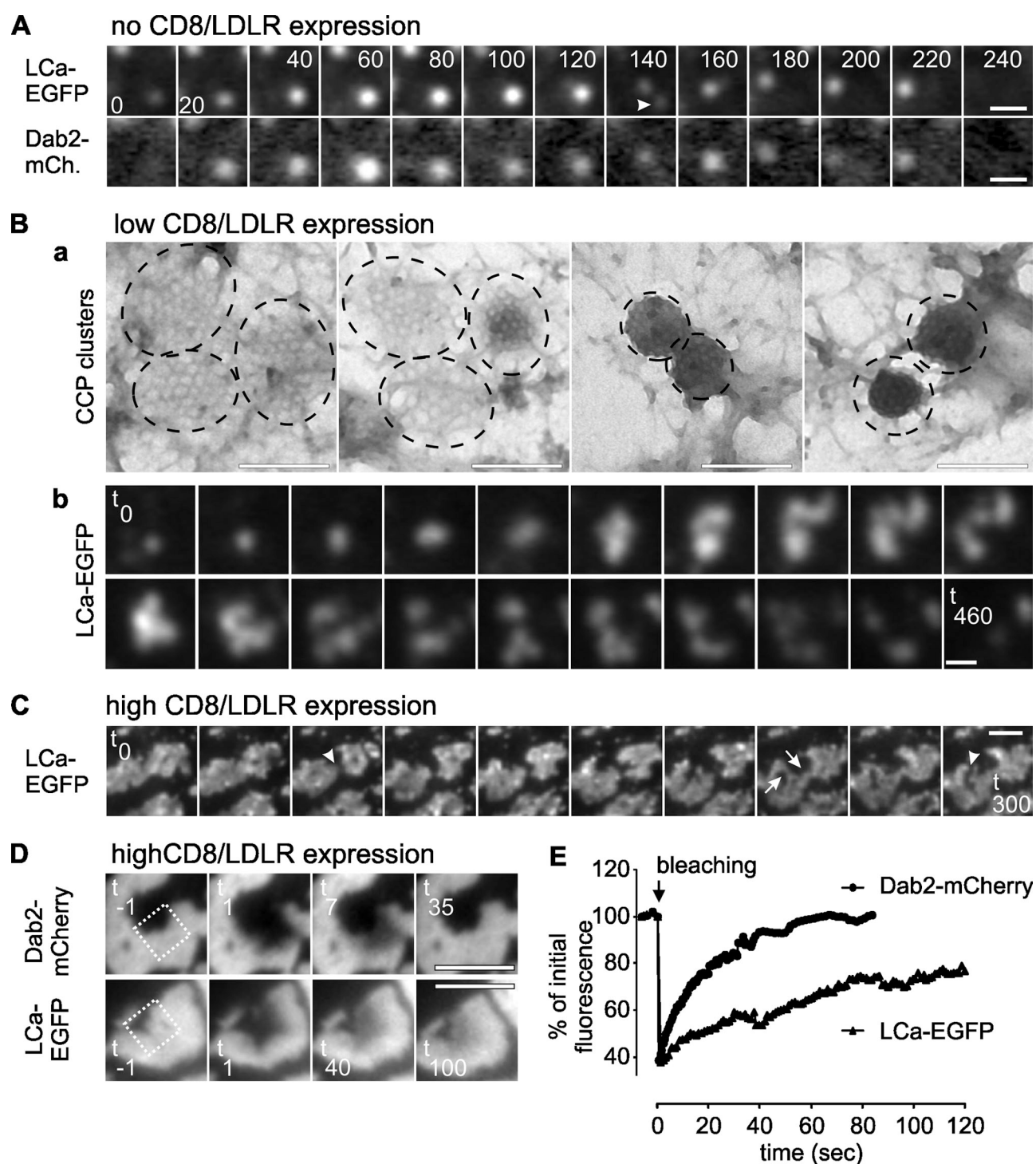


Figure 3. GCCSs are dynamic and, at moderate CD8/LDLR levels, generate nonterminal endocytic events. BSC1 cells were cultured as described in Fig. 1 and observed by dual-color TIRF-FM (A, Bb, C), electron microscopy (Ba), or spinning disk confocal microscopy (D). (A) Montage shows lifetime of a CCP. Arrowhead indicates nonterminal event. (B) In the presence of mild CD8/LDLR expression, CCPs tend to cluster and undergo nonterminal endocytic events. (C) GCCSs are dynamic and change morphology. (D) A small area in GCCSs has been bleached (indicated by square) and FRAP was recorded and quantified. Bars: (A) 400 nm; (Ba) 200 nm; (Bb) 600 nm; (C and D) 2 μ m.

(Stewart, 2007). ARH lacks a recognizable NLS, suggesting that an additional factor might be involved in its nuclear shuttling. To investigate whether nuclear export of ARH was an active process, we treated cells with leptomycin B (LmB), a potent inhibitor of nuclear exit. LmB prevented adenoviral-mediated CD8/LDLR expression (Fig. S3, D and E), and hence indirectly

inhibited ARH export (Fig. S3 Fa). However, if we first expressed CD8/LDLR for 2–7 h and then added LmB, ARH redistributed from the nucleus to CCPs (Fig. S3 Fb,c). Together, these results show that nuclear exit of ARH is passive and suggest the existence of a second PTB domain binding partner required for nuclear import of ARH. In this scenario, overexpression of

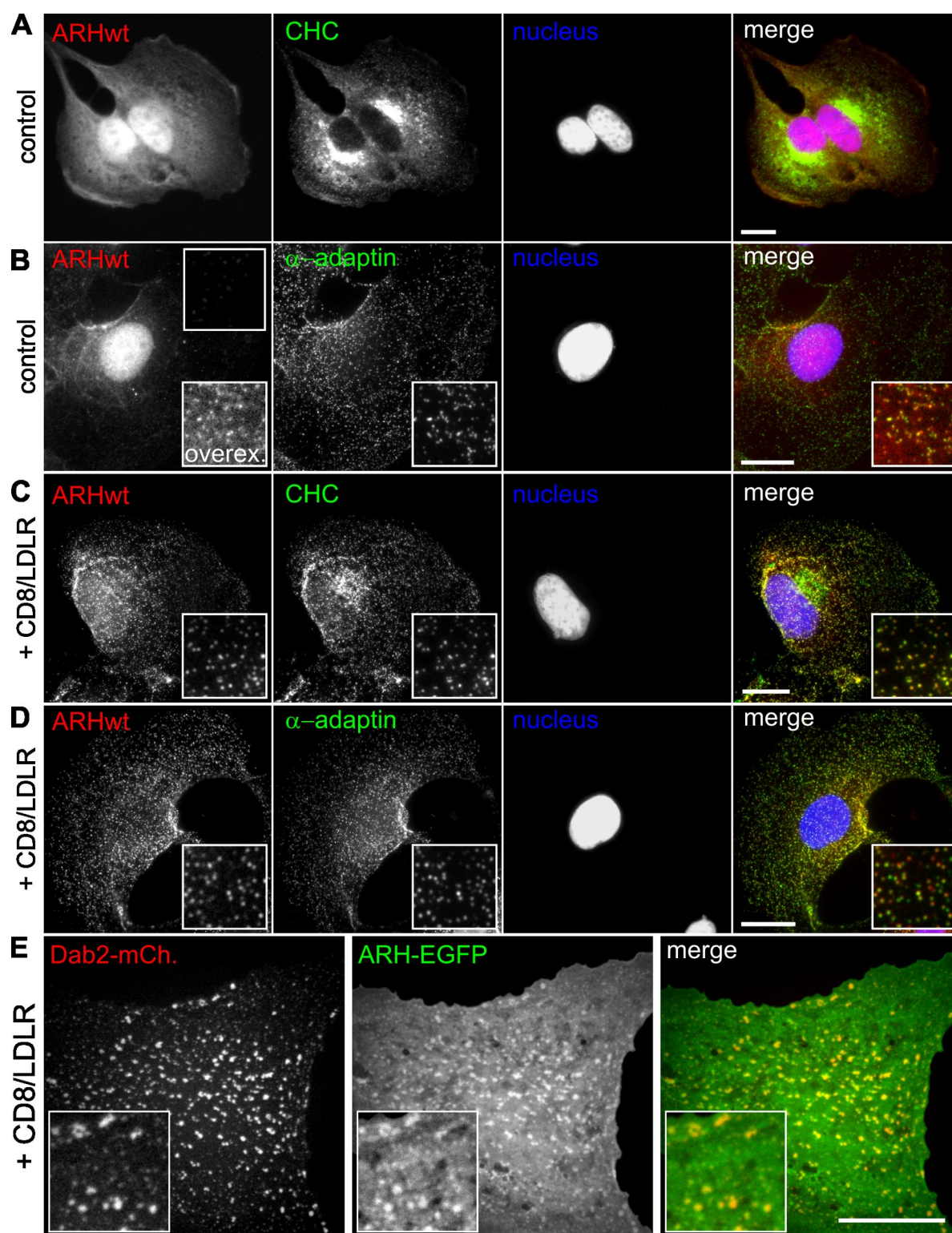


Figure 4. ARH localization is cargo dependent. BSC1 cells stably expressing ARH-mCherry were infected with adenoviruses coding for CD8/LDLR and cultured in the presence (A and B) or absence (C and D) of tet. Cells were then fixed, permeabilized, immunolabeled as indicated, and observed by epifluorescence. Insets show enlarged areas. (E) BSC1 cells coexpressing Dab2-mCherry, ARH-EGFP, and CD8/LDLR were fixed and visualized by spinning disk confocal microscopy. Bars, 10 μm.

the CD8/LDLR chimera might displace this factor and enable recruitment of ARH to the plasma membrane. Other endocytic adaptors, including epsin and β -arrestin (Pilecka et al., 2007) are known to shuttle to the nucleus, and Dab2 has been shown

to modulate LDLR expression (Eden et al., 2007). Therefore, although beyond the scope of this study, it will be worthwhile in future studies to explore the mechanisms governing ARH nuclear shuttling and the possible nuclear function of ARH.

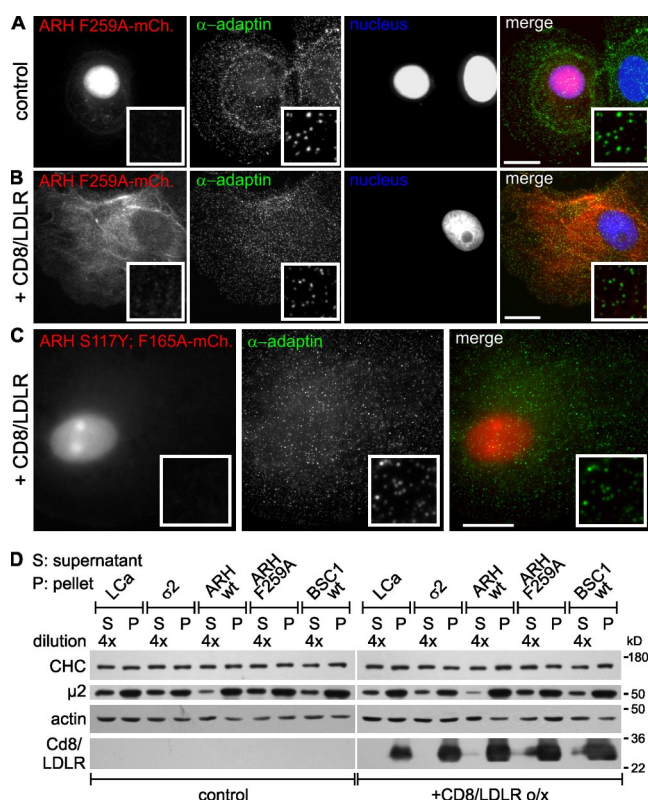


Figure 5. Requirements for ARH targeting to CCPs. BSC1 cells stably expressing ARH F259A-mCherry (A and B) or ARH S117Y;F165A-mCherry (C) were left untreated (A) or infected with adenoviruses coding for CD8/LDLR (B and C). Cells were then fixed, permeabilized, immunolabeled as indicated, and observed by epifluorescence. Bars, 10 μ m. (D) Indicated cell lines were cultured as previously described and analyzed by Western blot after subcellular fractionation. S: cytosolic fraction (diluted 4x); P: membrane fraction. Actin served as loading control. The cell fractionation experiment has been repeated at least three times and a typical experiment is shown.

ARH stabilized AP2 at the plasma membrane

Consistent with results from others (Mishra et al., 2005; Keyel et al., 2006, 2008; Maurer and Cooper, 2006), our data suggest that ARH recruitment to CCPs was dependent on AP2 interaction. Interestingly, we found that ARH expression induced strong membrane recruitment of AP2 even in the absence of CD8/LDLR overexpression (Fig. 5 D, μ 2 signal), indicating that a small amount of membranous ARH (Fig. 4 B, insets) is sufficient to increase CCP recruitment of AP2. Upon CD8/LDLR overexpression, the cytosolic pool of μ 2 was further depleted (Fig. 5 D) and as expected, the ARH-F259A mutant failed to increase AP2 membrane recruitment (Fig. 5 D). All other cell clones showed only slightly reduced or unchanged cytosolic pools of μ 2 upon CD8/LDLR overexpression, and the distribution of CHC between cytosol and the membrane fraction (i.e., ratio of 4:1) was unaffected (Fig. 5 D). Consistent with this, CD8/LDLR overexpression alone does not significantly alter overall CCP density (Fig. S4 A). Together, these results demonstrate a strong CD8/LDLR-dependent membrane recruitment of both ARH and AP2 that, because CCP density does not change, results in a cargo-dependent increase of the adaptor protein content per CCP.

ARH partially rescues saturated CME in an AP2-dependent manner

Previously, it has been reported that constitutive CME is saturable (Warren et al., 1997, 1998; Loerke et al., 2009). We confirmed this property in BSC1 cells by biochemically measuring CD8/LDLR endocytosis. Although total levels of internalized CD8/LDLR increase upon overexpression, a significant decrease in efficiency of endocytosis is apparent when cargo uptake is normalized to the total number of surface-expressed receptors. With increasing expression levels of CD8/LDLR, the efficiency of CME decreased (Fig. 6 A). To test whether this saturation reflected decreased efficiency of adaptor-mediated cargo clustering, we compared CD8/LDLR uptake in control cells with cells expressing one of various fluorescently tagged clathrin-coat components (i.e., LCa-EGFP, σ 2-EGFP, ARH-wt-mCherry, or ARH-F259A-mCherry). As expected, neither LCa-EGFP nor σ 2-EGFP expression increased uptake efficiency of CD8/LDLR chimeras (Fig. 6, B and C). However, the endocytic efficiency of CD8/LDLR uptake under high (0 ng/ml tet) expression levels was increased in cells expressing an additional pool of ARH (Fig. 6, B and C; open symbols/bars). To establish the specificity of this effect, we showed that TfR uptake, which was also saturated upon its overexpression, was not rescued by ARH (Fig. S1 C). The partial rescue of saturated CD8/LDLR uptake in cells expressing wt ARH-mCherry coincided with an \sim 48% decrease in the amount of extracellularly exposed CD8/LDLRs (unpublished data). This was expected because the amount of CD8/LDLRs at the membrane reflects the balance between endocytosis and recycling (the latter was unaffected by CD8/LDLR expression; unpublished data). Although endocytosis of CD8/LDLRs was more efficient with increased amounts of ARH, the rescue was incomplete, indicating the existence of other rate-limiting components during uptake of high CD8/LDLR loads.

As predicted by our previous findings, the endocytic efficiency of CD8/LDLR uptake in BSC1 cells was directly linked to the capability of ARH to bind AP2. Analysis of mutant ARH proteins defective in AP2 binding (Mishra et al., 2005) showed that expression of ARH-252A255, which has reduced ability to bind AP2, only slightly increased the efficiency of CD8/LDLR uptake, whereas expression of ARH-F259A, which is unable to bind AP2, had no effect (Fig. 6 C). Finally, depletion of AP2 through siRNA-mediated knockdown of μ 2 by 80% (unpublished data) ablated the ability of ARH-mCherry expression to restore the efficiency of CD8/LDLR endocytosis at high levels of expression (Fig. 6 C). Altogether, these data clearly establish the requirement of AP2 for ARH-mediated LDLR uptake, which mirrors the requirements for ARH targeting to CCPs. Furthermore, these results demonstrate that saturated CME can be partially accounted for by a limited amount of adaptor proteins.

Cargo overexpression prolongs the lifetime of productive CCPs

To better understand the role of the LDLR/ARH cargo-adaptor complex in regulating early stages in CME, we recorded time-lapse movies of LCa-EGFP-labeled CCPs in the presence or absence of CD8/LDLRs and/or ARH by TIR-FM and applied

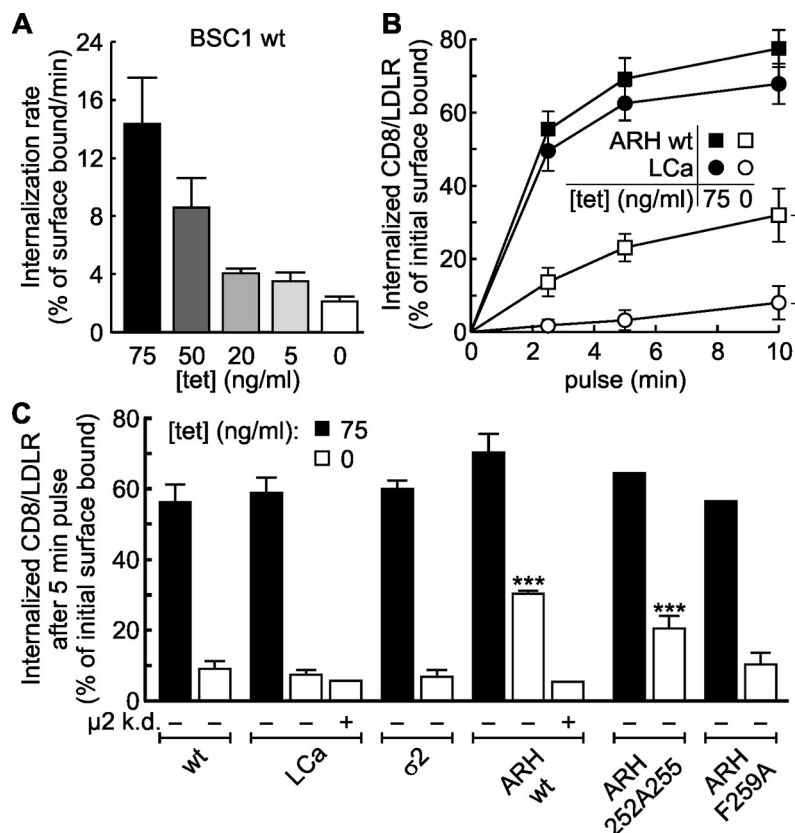


Figure 6. ARH partially rescues saturated LDLR uptake. (A) BSC1-wt cells infected with adenovirus coding for CD8/LDLR were cultured in the presence of the indicated concentrations of tet and the rate of anti-CD8 antibody internalization relative to surface bound ligand was measured at 37°C, as described in Materials and methods. (B) Time course of single round internalization of prebound anti-CD8 antibody in BSC1 cells expressing EGFP-CLCa (○, ●) or mCherry-ARH (□, ■). Shown are means (±SD) of at least three independent experiments. (C) BSC1-wt cells or cells stably expressing LCa-EGFP, α2-EGFP, ARH-wt, ARH-F259A, or ARH-252A255-mCherry were treated (+ μ2 k.d.) or not with μ2 siRNA to reduce AP2 levels, infected with CD8/LDLR adenovirus, and incubated with or without tet as indicated. The mean efficiency CD8/LDLR uptake as determined in at least two independent experiments is shown. Of note: to follow basal endocytic uptake of CD8, minimal exogenous expression of CD8/LDLR was necessary (i.e., overnight culture in the presence of 75 ng/ml tet). ***, confidence levels of $P < 0.001$ relative to wt control, 0 tet.

automated analysis of CCP trajectories as described previously (Jaqaman et al., 2008; Loerke et al., 2009). We were unable to follow CD8/LDLR clustering directly because overexpression of this chimera led to a strong decrease of the signal-to-noise ratio at the plasma membrane (Fig. S1 B), impeding automated tracking of cargo-laden CCPs.

As previously shown in control cells (Mettlen et al., 2009), productive CCPs, which ultimately lead to vesicle formation, contribute $50.7 \pm 2.0\%$ (mean ± jackknifed cell-to-cell error; Thomson and Chave, 1991) to the total number of CCPs found at the plasma membrane (Fig. 7 A), with early and late abortive CCPs representing $30.7 \pm 1.3\%$ and $17.0 \pm 1.3\%$, respectively. The remaining persistent CCPs ($1.7 \pm 0.4\%$; Fig. S4 B) failed to turn over for the duration of the 10-min movies. The calculated mean lifetimes were 5.7 ± 0.3 s, 19.1 ± 1.7 s, and 62.8 ± 3.1 s for early abortive, late abortive, and productive CCPs, respectively (Fig. 7 B).

Surprisingly, in cells overexpressing CD8/LDLRs in either the absence or presence of an additional pool of ARH, the relative contribution of productive CCPs decreased to $41.3 \pm 2.1\%$ and $44.5 \pm 2.2\%$, respectively (Fig. 7 A). This decrease in CCP maturation efficiencies was in contrast to our previously reported results upon TfnR overexpression (Loerke et al., 2009). To test whether this observation was due to an increased absolute number of abortive structures, and/or a decreased absolute number of productive CCPs, we measured the initiation density of CCPs (i.e., their rate of appearance per unit of cell surface). The average initiation rate of LCa-EGFP-labeled CCPs with lifetimes of 35–135 s (i.e., productive CCPs) was unaffected

by CD8/LDLR and/or ARH expression (control: 0.088 ± 0.026 pits/min/μm²; +CD8/LDLR: 0.089 ± 0.028 pits/min/μm²; +CD8/LDLR +ARH: 0.089 ± 0.025 pits/min/μm²; Fig. S4 C), whereas the initiation density of short-lived structures with lifetimes of 3–30 s (i.e., abortive CCPs; Fig. 7 B) increased (control: 0.29 ± 0.071 pits/min/μm²; +CD8/LDLR: 0.41 ± 0.093 pits/min/μm²; and +CD8/LDLR +ARH: 0.30 ± 0.066 pits/min/μm²). Together, these data indicate that CD8/LDLR overexpression stimulates initiation of CCPs, but does not affect the total number of productive CCPs. Thus, the reduced overall CCP maturation efficiency reflects an increased presence of abortive events.

Consistent with the decreased efficiencies of CME observed biochemically, the average lifetime of productive CCPs, which reflects the rate of maturation, increased significantly from 62.8 ± 3.1 s to 75.5 ± 5.0 s upon CD8/LDLR overexpression (Fig. 7 B). An additional pool of ARH did not alter the lifetimes of productive CCPs (76.3 ± 5.2 s), despite increasing the efficiency of CD8/LDLR endocytosis (Fig. 6 B). These data suggest that ARH expression enhances CD8/LDLR uptake by increasing packaging, i.e., the number of CD8/LDLRs per CCP and/or the size of CCPs, rather than by enhancing either the efficiency or rate of CCP maturation. In contrast to the effects on productive CCPs, the average lifetime of late abortive structures was decreased from 19.1 ± 1.7 s under control conditions to 15.5 ± 0.8 s upon expression of ARH (Fig. 7 B). Thus, CD8/LDLR overexpression together with its adaptor ARH lead to increased rates of initiation and turnover of abortive species.

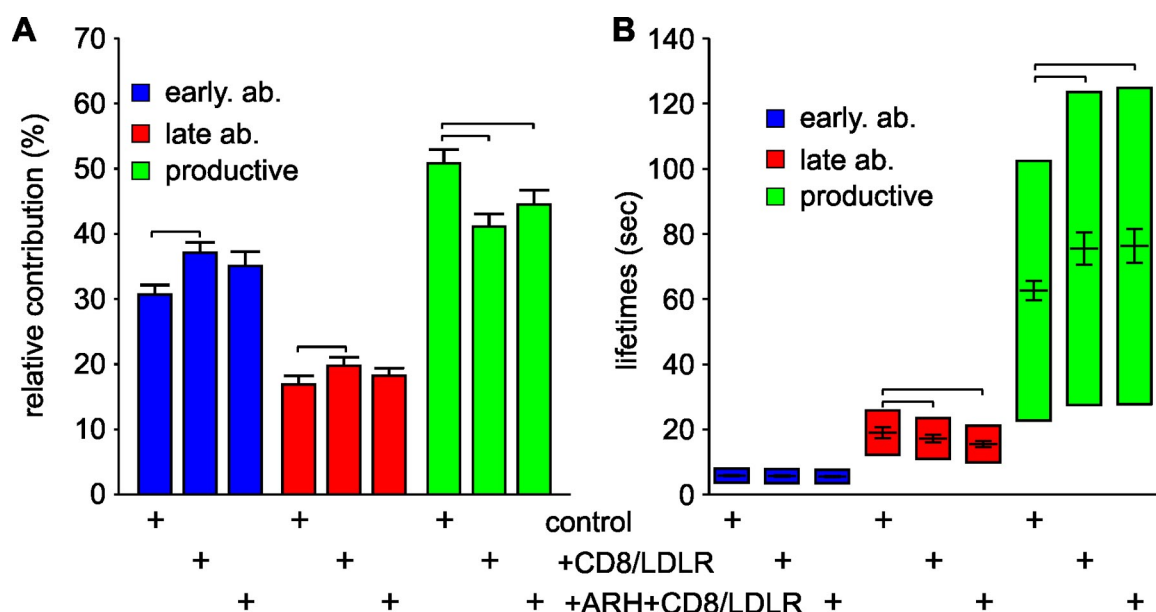


Figure 7. CD8/LDLRs prolong the lifetimes of productive CCPs. (A) TIR-FM time-lapse movies have been recorded and analyzed as described previously (Loerke et al., 2009). (A) Relative contributions and (B) lifetimes of CCP subpopulations labeled by LCa-EGFP are shown. Error bars represent cell-to-cell variation; the height of the lifetime bars in B denotes the range around the mean lifetime that contains 50% of the data. Brackets indicate confidence levels $P < 10^{-8}$ (Kolmogorov-Smirnov test). The number of CCP trajectories (n) and cells (k) for each condition are: LCa-EGFP control ($n = 100,823$; $k = 65$); LCa-EGFP + CD8/LDLR ($n = 70,955$; $k = 38$); LCa-EGFP + ARH + CD8/LDLR ($n = 23,394$; $k = 17$).

These effects suggest that additional factors, required to stabilize productive CCPs, become limiting during saturated CME.

CD8/LDLRs increase the amount of coat components per CCP

To further test the possibility that CD8/LDLR overexpression alters the size and/or packaging efficiency of CCPs, we extracted LCa-EGFP intensity profiles of CCP cohorts with a given lifetime range. These profiles are a general indicator of CCP growth and an indirect size measurement for structures under the light-diffraction limit (Saffarian and Kirchhausen, 2008).

Under control conditions (Fig. 8 A, blue lines), intensity profiles of LCa-EGFP-labeled CCPs were asymmetrically shaped, with the exception of the 10–20-s cohort, containing mainly abortive structures. We detected four phases of CCP maturation: (i) an initial phase of rapid growth, lasting ~ 30 s, during which CCPs of all lifetime cohorts acquired LCa-EGFP molecules (triskelia) with similar kinetics, (ii) an intensity plateau, (iii) a phase of slow intensity decline, and (iv) the rapid disappearance of the fluorescent signal. The maximum fluorescent intensities of LCa-EGFP at the plateau phase increased with lifetimes (Fig. 8 C, blue bars). CD8/LDLR overexpression strongly increased the intensities of all CCP cohorts (Fig. 8 A, red lines; Fig. 8 C, red bars) through an increased growth rate during the now slightly prolonged initial phase. The increase in growth corresponds to increased lifetimes of productive CCPs observed upon CD8/LDLR overexpression. Introduction of an additional pool of ARH (Fig. 8 B, green lines) further increased the intensities of LCa-EGFP signals, especially of those pits with lifetimes of 40–100 s (Fig. 8 C, green bars), consistent with CCP size measured by EM (Table I, Fig. S4 D). Together, these data establish that CD8/LDLR overexpression increases the size of CCPs,

and ARH enhances this effect and increases the packaging efficiency of CD8/LDLR into these enlarged CCPs.

In cells expressing CD8/LDLR, ARH-mCherry displayed nearly identical accumulation kinetics during the first 30–40 s at CCPs as compared with LCa-EGFP (Fig. 8 D, orange lines vs. green lines, respectively). However, ARH accumulation seemed to reach its maximum in CCPs with lifetimes > 80 s, whereas clathrin intensities were higher in longer-lived cohorts. Thus, CCPs that take longer to pinch off have a higher ratio of clathrin:ARH than shorter-lived CCPs. In addition, although the relative intensities of these two markers could not be directly compared, an earlier decrease of the ARH-mCherry signals compared with LCa-EGFP signals (Fig. 8 D, arrows) led to a more symmetrical shape of the ARH-mCherry profiles. A similar dissociation/redistribution has been suggested for AP2 (Rappoport et al., 2005; Saffarian and Kirchhausen, 2008) and was further supported by our analysis of CCP cohorts labeled by $\sigma 2$ -EGFP. Like LCa-EGFP and ARH-mCherry, AP2 rapidly accumulated in CCPs (Fig. 8 E, blue lines). However, unlike clathrin, but as for ARH-mCherry, these $\sigma 2$ -EGFP intensities began to decrease before LCa-EGFP. The apparently earlier disappearance of adaptors relative to clathrin indicates either their dissociation from CCPs before clathrin and/or a non-uniform redistribution of both ARH and AP2 in the clathrin lattice, resulting in their differential illumination within the TIRF field.

CD8/LDLR overexpression also increased signal intensities of all $\sigma 2$ -EGFP-labeled CCP cohorts (Fig. 8, E and F; red lines and bars, respectively) and prolonged the growth phase to ~ 50 s. Expression of an additional pool of ARH in the presence of CD8/LDLR reduced the amount of $\sigma 2$ -EGFP per CCP (Fig. 8, E and F; green lines and bars, respectively). Together, these data indicate that despite the dependence of ARH on AP2, these adaptors nonetheless also compete for incorporation into CCPs

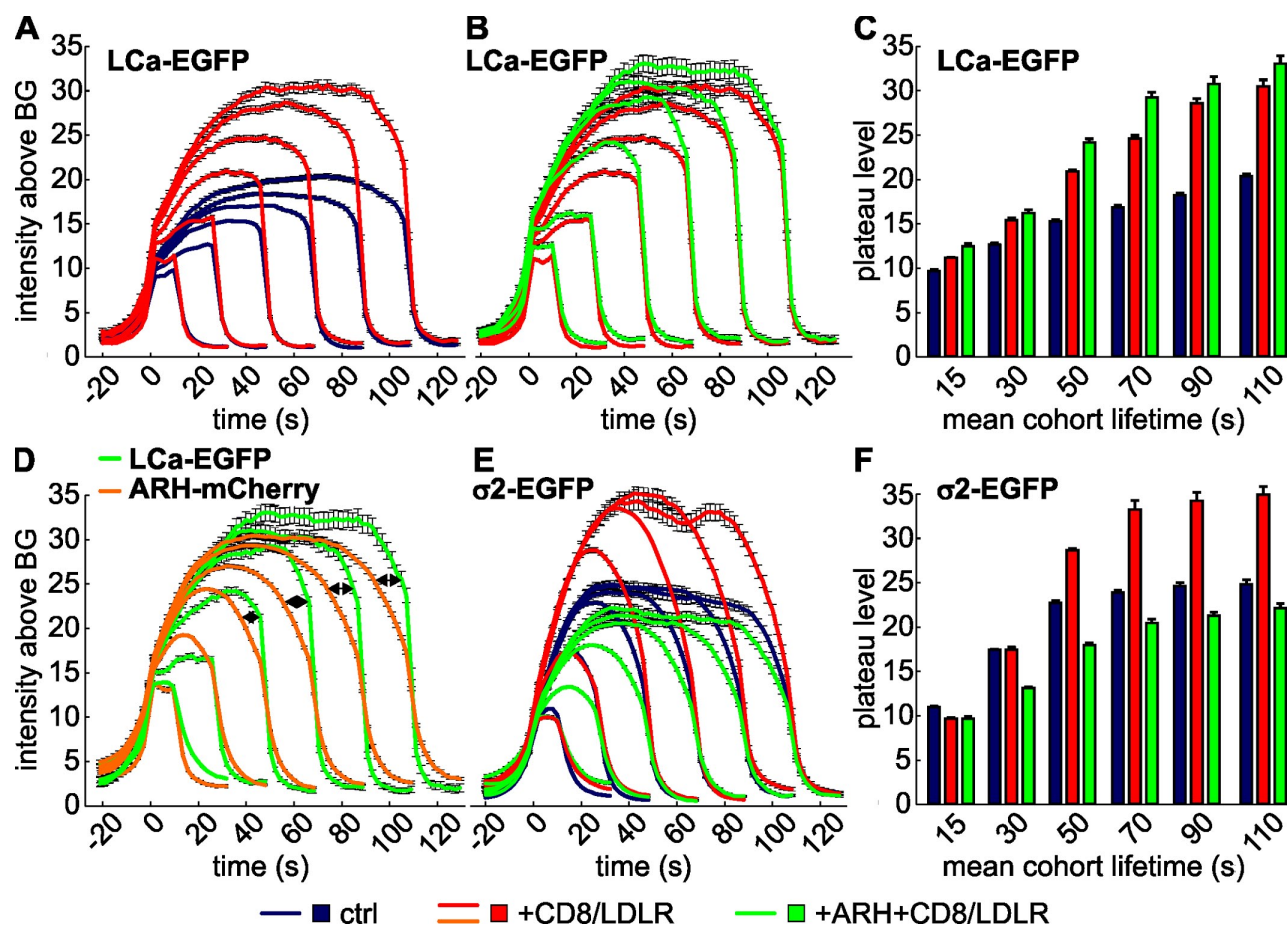


Figure 8. **CD8/LDLR and adaptors affect CCP size.** TIR-FM time-lapse movies have been recorded under various conditions, following the indicated fluorescently tagged protein. CCP cohorts of given lifetimes have been binned and their intensity profiles (A, B, D, and E) determined as a measure for CCP growth. The number of CCP trajectories for each condition, which ranges from 626 to 20,000, is shown in Table S1. The maximum plateau level of the LCa-EGFP (C) or σ 2-EGFP (F) is plotted against the mean cohort lifetime for the indicated cells.

and that the relative amounts of ARH and AP2 define the size (i.e., the intensities) of diffraction-limited CCPs.

Discussion

We have used a combination of immunofluorescence, biochemistry, electron microscopy, live-cell imaging by TIR-FM, and automated analysis of CCP trajectories to characterize how cargo and adaptor-specific mechanisms regulate CME. Previously, we showed that overexpression of TfnR, a constitutively internalized, AP2-dependent cargo, increased the efficiency of CCP maturation by increasing the contribution of productive CCPs at the expense of abortive species without affecting the rate of CCP maturation, i.e., the lifetimes of productive CCPs (Loerke et al., 2009). In contrast, we show here that overexpression of another constitutively internalized cargo, the LDLR, increases the rate of initiation and turnover of abortive CCPs, slows the rate of CCP maturation, and increases the size of CCPs through membrane recruitment of its specific adaptors, Dab2 and ARH. Together, these data strongly suggest that the observed heterogeneity in the dynamic behavior of CCPs (Merrifield et al., 2005; Rappoport et al., 2005; Yazar et al., 2005) could reflect differences in their content of cargo and adaptor molecules.

Dab2 and ARH are differentially recruited to CCPs, yet compete for occupancy

In agreement with previous studies (Morris and Cooper, 2001; Keyel et al., 2006; Maurer and Cooper, 2006; Chetrit et al., 2009), we observed colocalization of exogenously expressed mCherry-labeled Dab2 with clathrin-coat components in control cells. Under the same experimental conditions, ARH displayed a fundamentally distinct intracellular distribution: it was predominantly nuclear with only a barely detectable recruitment to CCPs. ARH can interact directly with both clathrin (He et al., 2002) and AP2 complexes (Mishra et al., 2005); hence, the absence of ARH from CCPs under control conditions suggests that ARH recruitment is highly regulated and involves a yet-unidentified factor/mechanism. This hypothesis is strongly supported by the observation that (i) ARH translocated from the nucleus into the cytosol upon CD8/LDLR expression, and (ii) this nucleo-cytoplasmic shuttling did not depend on AP2 binding and/or CCP recruitment, but on a functional PTB domain.

Dab2 and ARH compete with each other and with AP2 for binding sites within the same CCPs as evidenced by (i) the strong colocalization of these various adaptors in CCPs, (ii) the competition of ARH and Dab2 for cargo binding, thereby disrupting Dab2 scaffolding of GCCs, and (iii) the displacement of AP2

by ARH from cargo-laden CCPs. Overexpression of a specific receptor and its adaptors alters the relative adaptor composition of CCPs and hence their dynamic behavior. There has been some controversy as to whether TfnR and LDLR can be co-internalized in a single CCP (Keyel et al., 2006; Lakadamyali et al., 2006). Our data are consistent with the ability of CCPs to take up multiple distinct receptors. However, we speculate that cargo-specific mechanisms (e.g., ligand-induced receptor clustering) could, under steady-state conditions, alter the relative proportions of specific receptors and their adaptors to specifically affect the properties of individual CCPs. Such effects have been observed for G protein-coupled signaling receptors (Puthenveedu and von Zastrow, 2006).

ARH is AP2 dependent and limiting during CD8/LDLR uptake

Although biochemical measurements establish that CD8/LDLR endocytosis is saturable, resulting in a markedly decreased efficiency of CME, the effect of CD8/LDLR overexpression on CCP dynamics was relatively small. This apparent discrepancy reflects the fact that biochemical assays for ligand uptake measure CME indirectly and the efficiency of CME depends on cargo loading/concentration into CCPs. At very high levels of expression, most of the CD8/LDLRs are diffusely distributed on the plasma membrane and not captured in CCPs. In contrast, the TIRF-based assays measure CCP dynamics and CCV formation directly. That these kinetics were less affected by CD8/LDLR overexpression argues that reduced CME efficiency under these conditions reflects saturation of adaptor-dependent recruitment of cargo into CCPs.

Previous studies have reported a strong inhibition of fluorescent DiI-LDL internalization after transient expression of ARH-GFP in HeLa cells (Mishra et al., 2005). Here, we have taken care to select stable transformants expressing low levels of ARH-mCherry and show biochemically that ARH is able to increase the efficiency of LDLR uptake at saturation. This activity was dependent on its abilities to bind LDLR through its PTB domain and to interact with AP2. Increased efficiency of LDLR uptake upon ARH expression was not achieved through an increased CCP density, an increased percentage of productive CCPs, or an increased rate of their maturation. Instead, it occurred through an increased efficiency of LDLR sorting/packaging into CCPs. Our live-cell and electron microscopy experiments demonstrated that this is accomplished, in part, by a prolonged growth phase and increased size of individual CCPs.

CD8/LDLRs and their adaptors increase the size and dynamic behavior of productive CCPs

In contrast to TfnR overexpression, which did not affect AP2 distribution (Loerke et al., 2009), overexpression of CD8/LDLR increased the recruitment of both Dab2 and ARH to the plasma membrane. This recruitment of adaptor proteins had differential effects on CCP size and their dynamic behaviors.

In cells expressing Dab2-mCherry, the size of CCPs increased with increasing levels of CD8/LDLR expression. At endogenous levels of cargo, we observed an increase in the number of nonterminal endocytic events, suggesting that under these conditions, larger CCPs assemble so that a residual clathrin patch

remains after CCV budding. The number of nonterminal events increased upon mild overexpression of cargo, and clusters of dynamic CCPs were observed. The presence or absence of a variable fraction of nonterminal events in different cell types could be explained by variable amounts of cargo and/or Dab2 at the plasma membrane. This idea is further supported by the observation that nonterminal events are more frequent in HeLa cells (Ehrlich et al., 2004; Merrifield et al., 2005; Loerke et al., 2009), which express relatively high levels of Dab2 and cargo (Maurer and Cooper, 2006; unpublished data). At very high levels of CD8/LDLR overexpression, Dab2 induced the formation of large, flat, and endocytically inactive clathrin lattices on the ventral cell surface. Similar GCCSs have been observed in other cell types upon Dab-2 overexpression, associated with integrins, another Dab2-specific cargo molecule (Chetrit et al., 2009). Hence, GCCS formation is likely dependent on levels of expression of Dab2 and endogenous cargo. We speculate that the cargo-dependent recruitment of Dab2 contributes to a more extended adaptor scaffold at the plasma membrane, thereby guiding—presumably through its NPF motifs—recruitment of additional endocytic accessory proteins that affect the extent of clathrin polymerization and the dynamic behavior of CCPs.

When CD8/LDLR and ARH were coexpressed, CCPs also grew in size, as detected by increased clathrin intensities and electron microscopy, yet they remained under the light-diffraction limit. Thus, we observed a cargo and adaptor expression-dependent continuum in regulating the size of CCPs, such that TfnR overexpression < control cells = Dab2 alone < CD8/LDLR overexpression alone < low CD8/LDLR + Dab2 < high CD8/LDLR + ARH << high CD8/LDLR + Dab2. The fact that both Dab2 and ARH increased the size of CCPs relative to CCPs in which AP2 is the predominant adaptor (i.e., under conditions of TfnR overexpression) might reflect the need to accommodate the very large ligands bound by LDLR and LRP (Jones et al., 2003) (i.e., LDL particles, $d \sim 22$ nm and $\alpha 2$ -macroglobulin, $d \sim 18.5$ nm; Krimbou et al., 1998), respectively. Additional studies are required to determine the molecular mechanisms controlling the extent of clathrin polymerization.

Adaptor content and the endocytosis checkpoint

We previously identified an endocytic restriction/checkpoint and provided evidence that progression beyond the checkpoint (i.e., CCP maturation efficiency) was enhanced by TfnR overexpression in a manner dependent on AP2 adaptors (Loerke et al., 2009). Subsequently, we identified a subset of endocytic accessory factors, including membrane curvature and coat-sensing proteins, whose siRNA knockdown altered the rate and extent of turnover of abortive CCPs (Mettlen et al., 2009). These data suggested that factors recruited to AP2 complexes through interactions with their appendage domains might provide input into the endocytic checkpoint.

Although much work remains to test this checkpoint hypothesis and its implications and mechanisms, the results reported here provide some new insight as to how the checkpoint might respond to cargo content and adaptor assembly. For example, in contrast to the effects of TfnR overexpression, increased

LDLR/ARH levels led to a slight increase in the initiation, turnover rate, and number of abortive CCPs. Under these conditions, ARH partially displaces AP2 from CCPs, which could account for the destabilization of nascent CCPs. Dab2, unlike ARH, is recruited to CCPs and can function independently of AP2. Thus, the Dab2-dependent formation of nonfunctional, flat GCCSs under conditions of high cargo concentrations could reflect an imbalance of protein–protein interactions, possibly involving the disproportionate recruitment, through the multiple NPF motifs found in Dab2, of EH domain-containing proteins (e.g., Eps15, Eps15R, and intersectin) that bind directly or indirectly to clathrin. This could potentially bypass the requirement for a threshold amount of AP2 and its associated partners, and hence disrupt signaling to the endocytic restriction/checkpoint. This hypothesis is supported by the observations that in the presence of CD8/LDLR: (i) Dab2-p67, which is unable to bind clathrin and AP2 but contains NPF motifs, was able to induce the formation of GCCSs; (ii) ARH, which is lacking NPF motifs, did not induce formation of flat lattices; (iii) a mix of ARH and Dab2 led to the breakdown of GCCSs; and (iv) AP2 complexes are nonuniformly distributed in GCCSs.

Altogether, our results underscore the highly dynamic and cargo-responsive nature of clathrin coats and illustrate the complexity of CCP maturation. Together with our previous results (Loerke et al., 2009), we establish that even constitutively internalized cargo and their adaptors can regulate multiple aspects of CCP maturation and that variations in adaptor/cargo content can account, in part, for the dynamic heterogeneity of CCPs.

Materials and methods

Cell lines and cell culture

BSC1 cells stably expressing rat brain clathrin light chain α -EGFP (LC α -EGFP) or the AP2 rat brain α 2-adaptin fused to EGFP were provided by Dr. T. Kirchhausen (Harvard Medical School, Boston, MA). All cells were grown under 5% CO₂ at 37°C in DME supplemented with 20 mM Hepes, 10 mg/ml streptomycin, 66 μ g/ml penicillin, and 10% (vol/vol) fetal calf serum (HyClone). Cells stably expressing fluorescently tagged proteins were cultured in the continuous presence of 0.5 mg/ml geneticin.

Preparation of plasmids, viruses, and stable cell lines

cDNAs encoding Dab2 and ARH were provided by Linton Traub (University of Pittsburgh, Pittsburgh, PA). C-terminally tagged Dab2wt, Dab2-p67, ARHwt, ARH-F259A, ARH-252A255, and ARH-S117Y:F165A coupled to mCherry were made by first fusing the corresponding DNA (amplified by PCR) to the 3' end of the coding sequence for EGFP (pEGFP-C1; Takara Bio Inc.) and then replacing EGFP by mCherry. N-terminal myristoylated Dab2-mCherry was produced by cloning the fluorescently tagged protein into a pC4M-F2E expression plasmid (ARAD).

BSC1 monkey kidney cells stably expressing either wild-type or mutant forms of ARH were obtained by transfection of wild-type cells using Lipofectamine 2000 (Invitrogen) according to the manufacturer's recommendation and a 3-wk selection in DME supplemented with 10% fetal bovine serum and geneticin (1 mg/ml; Invitrogen).

siRNA treatment

μ 2 expression was depleted through siRNA treatment with RNA oligos (Thermo Fisher Scientific) targeting AAGUGGAUGCCUUUCGGGUCA (Motley et al., 2003). Cells were plated on 60-mm Petri dishes at a density of 8.3×10^3 cells/cm². After overnight incubation, cells were washed with Opti-MEM (Invitrogen) and transfected once with siRNA oligos (50 nM final concentration) using HiPerFect transfection reagent as a delivery agent (QIAGEN), according to the manufacturer's recommendations. Cells were placed in ordinary culture medium 8 h after transfection and processed for TIR-FM or Western blot analysis the next day.

Adenoviral infection, immunofluorescence, and TIR-FM

Cells were plated on glass coverslips (refractive index 1.523; Corning) at a density of 8.3×10^3 cell/cm² and co-infected with adenoviruses coding for the CD8/LDLR chimera and adenoviruses coding for a tet repressible transcription activator. After overnight incubation in the presence (1,000 ng tet/ml; control cells) or absence of tet (to allow CD8/LDLR overexpression), cells were washed three times in PBS and fixed in a mixture of prewarmed paraformaldehyde (2% final; Electron Microscopy Sciences) and Triton X-100 (0.5% final) for 2 min, then with paraformaldehyde (4% final) for an additional 18 min. Reactive aldehydes and nonspecific binding sites were quenched for 30 min with Q-PBS (PBS supplemented with 0.01% [wt/vol] saponin, 2% [wt/vol] BSA, and 0.1% [wt/vol] lysine, pH 7.4), then incubated at room temperature for 1 h in primary antibodies diluted in Q-PBS: anti- α -adaptin (clone 100/2; Sigma-Aldrich), anti- β -adaptin (clone 100/1; Sigma-Aldrich), anti-CD8 (clone UCHT4; Ancell), and anti-clathrin heavy chain (clone X22; Hybridoma). After extensive washing with Q-PBS, samples were incubated with the appropriate Alexa 488 (green) or -568 (red) secondary antibodies (Invitrogen) at 5 μ g/ml in Q-PBS supplemented or not with the nuclear stain DAPI (2.5 μ g/ml) for 1 h in the dark. For F-actin staining, cells were incubated with phalloidin-Alexa 488 (0.8 units/ml). Samples were washed, postfixed with 4% (wt/vol) paraformaldehyde for 5 min, and washed twice with PBS. Coverslips were then mounted in Fluoromount G (Electron Microscopy Sciences). Epifluorescence images of fixed cells were acquired on an inverted microscope (Axiovert 200M; Carl Zeiss, Inc.) coupled to a 14-bit cooled CCD camera (Cool SNAP HQ2; Photometrics) controlled by MetaMorph software (Universal Imaging Corp.), using a 63x/1.4 NA Plan Apo objective (Carl Zeiss, Inc.).

For live-cell TIR-FM imaging, cells were preincubated with imaging medium (DME, devoid of phenol red and containing 10 mM Hepes and 5% fetal bovine serum, pH 7.4). Coverslips were then mounted on a slide and rapidly transferred to a prewarmed microscope stage as described in Yarar et al. (2005). Five or six cells (i.e., movies) were recorded per coverslip in fast (frame rate 400 ms) and slow (frame rate 2 s) acquisition mode during 10 min, using a 100x 1.45 NA objective (Nikon) mounted on an inverted microscope (model TE2000U; Nikon) and a 14-bit mode operated camera (Orca II-ERG; Hamamatsu Photonics). The theoretical depth of the evanescent field (d) was <100 nm and exposure times were 80–90 or 180–200 ms, depending on the frame rate and the intensity of the signal.

FRAP was performed using an inverted microscope (model TE2000E; Nikon) in which the 488-nm and 568-nm line of a Kr/Ar laser (2.5 W; Spectraphysics) was introduced fiber-optically into a FRAP illuminator (Nikon) and images were collected with a 63x/1.4 NA Plan Apo DIC objective (Nikon) on a spinning-disk confocal scanner (Yokogawa) using an Orca ER camera (Hamamatsu Photonics); fluorescence recovery was imaged at 1-s intervals for 2 min. The intensity of each bleached region was measured using MetaMorph, corrected to the intensity of an unbleached region in the frame to account for any fluctuations in intensity, and then normalized to the average intensity of five frames before the bleach.

Automated image and CCP lifetime and intensity profile analysis

Fluorescent particle detection and life-time tracking of CCPs in the TIR-FM movies was accomplished using the software package described in Jaqaman et al. (2008). The lifetime analysis of CCPs was performed as described in Loerke et al. (2009) and P values were determined as in Mettlen et al. (2009). For the intensity profile analysis, we used the entirety of CCP trajectories to calculate averaged intensity time courses for conglomerates of CCPs within a given lifetime range (i.e., CCP cohorts). The averaging first aligned and averaged the common first time point of the intensity time courses (i.e., the point at which the trajectory is first detected), yielding the "appearance-aligned" average. The time courses were then aligned to their last time point (i.e., the last detected point of the trajectory) and averaged, yielding the "disappearance-aligned" average. The global average was calculated as the weighted combination of the appearance- and disappearance-aligned averages, weighted toward the appearance-aligned trace at the beginning and weighted toward the disappearance-aligned trace at the end. This procedure reduced noise by averaging, while preserving the fast intensity dynamics at the beginning and end of the trajectory. Finally, the maximum plateau levels of intensity profiles were determined by averaging the five highest intensity values in each trace.

Estimation of surface-bound/endocytic uptake of CD8/LDLR chimeras

Cells, plated in 10-cm dishes and co-infected with adenoviruses, were cultured in the absence (high CD8/LDLR overexpression) or presence of 75 ng/ml tet (very low CD8/LDLR expression). After overnight incubation, cells were

washed 3× in PBS, harvested in PBS containing 5 mM EDTA, pelleted in the presence of MgCl₂ (1 mM), and resuspended in 400 µl ice-cold PBS+ (1 mM CaCl₂, 1 mM MgCl₂, 0.2% BSA [wt/vol], and 5 mM glucose), and supplemented with biotinylated anti-human CD8 antibodies (clone UCGT4, 5 µg/ml final; Ancell) for 45 min (on ice) to allow binding, followed by three gentle washes in ice-cold PBS+ (resuspension/sedimentation) to remove nonbound antibodies. Aliquots of cells were either kept on ice and lysed as described below (to determine the amount of surface exposed CD8/LDLR chimera) or warmed to 37°C for the indicated times to measure endocytic uptake. Endocytosis was stopped by returning cells to ice and noninternalized CD8/LDLR chimera were masked by successive treatment with avidin and biocytin (Sigma-Aldrich). Finally, cells were lysed in blocking buffer (2% BSA [wt/vol], 1% Triton X-100 [vol/vol], 0.1% SDS [wt/vol], 1 mM EDTA, 50 mM NaCl, and 10 mM Tris-HCl, pH 7.4).

To measure surface-bound and intracellular CD8/LDLR chimera, known amounts of anti-human CD8 antibodies (standard curve) and cell lysates were loaded into 96-well ELISA plates (Thermo Fisher Scientific) coated with anti-mouse antibodies and incubated overnight at 4°C. After extensive washes with PBS and blocking buffer, plates were incubated with streptavidin/HRP conjugate (1:5,000; Roche) for 1 h. HRP activity was measured by a stopped colorimetric assay using ortho-dianisidine as a substrate. Light absorption at 490 nm was determined with a Bio-Stack microplate reader (Bio-Tek) and all values were corrected by light absorbance at 650 nm and normalized by the total cell protein content (bicinchoninic acid assay).

Cell fractionation and Western blotting

For Western blots, cells grown in 60-mm dishes were washed twice with PBS and harvested in PBS containing 5 mM EDTA. Protein concentration was determined and low speed cell pellets were gently resuspended in fractionation buffer (25 mM sucrose, 1 mM MgCl₂, 2 mM EGTA, and 25 mM Hepes, pH 7.4) to equal protein concentration—the lowest protein condition being resuspended in 300 µl. Cells were lysed by three cycles of freezing/thawing in liquid N₂ and equal volumes of whole-cell lysates were centrifuged at 110,000 g in a rotor (model TLA100.2; Beckman Coulter) for 30 min. The soluble fraction (cytosolic fraction “S”) was collected and pellets (membrane fraction “P”) were resuspended in 150 µl fractionation buffer and sonicated. The “S” fraction was further diluted 2× and equal volumes were separated by SDS-PAGE, transferred to a nitrocellulose membrane (GE Healthcare), blocked for 1 h in blocking buffer (20 mM Tris-base, 15 mM NaCl, 5 mM EDTA, 0.5% [vol/vol] Tween 20, and 5% [wt/vol] milk powder, pH 7.4), incubated overnight with primary antibodies at 4°C: clathrin heavy chain (TD1; Hybridoma), µ2 (AP50; BD), actin (clone C4; Millipore), and CD8 (clone H-169; Santa Cruz Biotechnology, Inc.), and revealed by HRP-labeled secondary antibodies and enhanced chemiluminescence.

Electron microscopy of ventral membrane surfaces

The ventral surfaces of unroofed cells were prepared for visualization by negative stain EM according to published procedures (Wilson et al., 2007). In brief, BSC1-wt (either transfected with Dab2-mCherry or infected with CD8/LDLR expressing adenovirus system or both) or BSC1 cells stably expressing ARH were seeded and cultured overnight on poly-L-lysine-coated EM grids. Cells were “unroofed” by applying a poly-L-lysine-coated coverslip, pressure, and then ripping off the EM grids and adherent ventral PM sheets as described previously (Wilson et al., 2007). These were rapidly fixed first in 2% PFA (20 min), then 2% glutaraldehyde (10 min), stained with uranyl acetate, and visualized on an electron microscope (model CM-100; Philips).

Online supplemental material

Fig. S1 shows that CD8/LDLR expression is regulated by tet and that TfnR overexpression saturates its endocytosis, which is not affected by ARH. Fig. S2 shows colocalization between Dab2 and AP2 upon overexpression of CD8/LDLR and TfnR, and that not all CCPs labeled with clathrin contain AP2. Fig. S3 shows the altered cell morphology and actin organization in ARH-mCherry-expressing cells and that leptomycin B blocks LDLR expression, but not subsequent nuclear exit of ARH. Fig. S4 shows data for CCP densities, initiation densities of productive CCPs, relative contributions of persistent CCPs in BSC1 cells under various conditions, and increased CCP sizes upon coexpression of CD8/LDLR and ARH. Video 1 shows that GCCSs (here labeled by LCa-EGFP) are exclusively found at the ventral plasma membrane. Video 2 shows CCP dynamics in cells expressing mCherry-Dab2. Video 3 shows multiple CCV internalization events from enlarged CCSs in BSC1 cells expressing Dab2 and moderate levels of CD8/LDLR.

Video 4 shows that AP2 forms dynamic clusters within enlarged CCSs in BSC1 cells expressing Dab2 and moderate levels of CD8/LDLR. Video 5 shows the dynamic behavior of GCCSs formed in BSC1 cells expressing Dab2 and high levels of CD8/LDLR. Online supplemental material is available at <http://www.jcb.org/cgi/content/full/jcb.200908078/DC1>.

We thank Vasyil Lukiyanchuk for preparation of cDNA constructs and lentiviruses, Malcolm Wood, Director of the TSRI Core EM facility, for EM sample preparation and imaging, Bridget Wilson and Mary Raymond-Stintz (University of New Mexico) for advice on EM, and members of the Schmid and Danuser laboratories for helpful discussions. This is TSRI manuscript number 20307.

This research was supported by National Institutes of Health RO1 grants (GM73165 to G. Danuser and S.L. Schmid, and MH61345 to S.L. Schmid), by a fellowship from the American Heart Association to M. Mettlen, and from the Leukemia and Lymphoma Society to D. Yazar.

Submitted: 17 August 2009

Accepted: 18 February 2010

References

- Arca, M., G. Zuliani, K. Wilund, F. Campagna, R. Fellin, S. Bertolini, S. Calandra, G. Ricci, N. Glorioso, M. Maioli, et al. 2002. Autosomal recessive hypercholesterolemia in Sardinia, Italy, and mutations in ARH: a clinical and molecular genetic analysis. *Lancet*. 359:841–847. doi:10.1016/S0140-6736(02)07955-2
- Brodsky, F.M. 1988. Living with clathrin: its role in intracellular membrane traffic. *Science*. 242:1396–1402. doi:10.1126/science.2904698
- Chetrit, D., N. Ziv, and M. Ehrlich. 2009. Dab2 regulates clathrin assembly and cell spreading. *Biochem. J.* 418:701–715. doi:10.1042/BJ20081288
- Davis, C.G., M.A. Lehrman, D.W. Russell, R.G. Anderson, M.S. Brown, and J.L. Goldstein. 1986. The J.D. mutation in familial hypercholesterolemia: amino acid substitution in cytoplasmic domain impedes internalization of LDL receptors. *Cell*. 45:15–24. doi:10.1016/0092-8674(86)90533-7
- Edeling, M.A., S.K. Mishra, P.A. Keyel, A.L. Steinhauser, B.M. Collins, R. Roth, J.E. Heuser, D.J. Owen, and L.M. Traub. 2006. Molecular switches involving the AP-2 beta2 appendage regulate endocytic cargo selection and clathrin coat assembly. *Dev. Cell*. 10:329–342. doi:10.1016/j.devcel.2006.01.016
- Eden, E.R., X.M. Sun, D.D. Patel, and A.K. Soutar. 2007. Adaptor protein disabled-2 modulates low density lipoprotein receptor synthesis in fibroblasts from patients with autosomal recessive hypercholesterolemia. *Hum. Mol. Genet.* 16:2751–2759. doi:10.1093/hmg/ddm232
- Ehrlich, M., W. Boll, A. Van Oijen, R. Hariharan, K. Chandran, M.L. Nibert, and T. Kirchhausen. 2004. Endocytosis by random initiation and stabilization of clathrin-coated pits. *Cell*. 118:591–605. doi:10.1016/j.cell.2004.08.017
- Garcia, C.K., K. Wilund, M. Arca, G. Zuliani, R. Fellin, M. Maioli, S. Calandra, S. Bertolini, F. Cossu, N. Grishin, et al. 2001. Autosomal recessive hypercholesterolemia caused by mutations in a putative LDL receptor adaptor protein. *Science*. 292:1394–1398. doi:10.1126/science.1060458
- Garuti, R., C. Jones, W.P. Li, P. Michaely, J. Herz, R.D. Gerard, J.C. Cohen, and H.H. Hobbs. 2005. The modular adaptor protein autosomal recessive hypercholesterolemia (ARH) promotes low density lipoprotein receptor clustering into clathrin-coated pits. *J. Biol. Chem.* 280:40996–41004. doi:10.1074/jbc.M509394200
- Hanover, J.A., L. Beguinot, M.C. Willingham, and I.H. Pastan. 1985. Transit of receptors for epidermal growth factor and transferrin through clathrin-coated pits. Analysis of the kinetics of receptor entry. *J. Biol. Chem.* 260:15938–15945.
- He, G., S. Gupta, M. Yi, P. Michaely, H.H. Hobbs, and J.C. Cohen. 2002. ARH is a modular adaptor protein that interacts with the LDL receptor, clathrin, and AP-2. *J. Biol. Chem.* 277:44044–44049. doi:10.1074/jbc.M208539200
- He, J., J. Xu, X.X. Xu, and R.A. Hall. 2003. Cell cycle-dependent phosphorylation of Disabled-2 by cdc2. *Oncogene*. 22:4524–4530. doi:10.1038/sj.onc.1206767
- Jaqaman, K., D. Loeke, M. Mettlen, H. Kuwata, S. Grinstein, S.L. Schmid, and G. Danuser. 2008. Robust single-particle tracking in live-cell time-lapse sequences. *Nat. Methods*. 5:695–702. doi:10.1038/nmeth.1237
- Jing, S.Q., T. Spencer, K. Miller, C. Hopkins, and I.S. Trowbridge. 1990. Role of the human transferrin receptor cytoplasmic domain in endocytosis: localization of a specific signal sequence for internalization. *J. Cell Biol.* 110:283–294. doi:10.1083/jcb.110.2.283
- Jones, C., R.E. Hammer, W.P. Li, J.C. Cohen, H.H. Hobbs, and J. Herz. 2003. Normal sorting but defective endocytosis of the low density lipoprotein receptor in mice with autosomal recessive hypercholesterolemia. *J. Biol. Chem.* 278:29024–29030. doi:10.1074/jbc.M304855200

- Keyel, P.A., S.K. Mishra, R. Roth, J.E. Heuser, S.C. Watkins, and L.M. Traub. 2006. A single common portal for clathrin-mediated endocytosis of distinct cargo governed by cargo-selective adaptors. *Mol. Biol. Cell.* 17:4300–4317. doi:10.1091/mbc.E06-05-0421
- Keyel, P.A., J.R. Thieman, R. Roth, E. Erkan, E.T. Everett, S.C. Watkins, J.E. Heuser, and L.M. Traub. 2008. The AP-2 adaptor beta2 appendage scaffolds alternate cargo endocytosis. *Mol. Biol. Cell.* 19:5309–5326. doi:10.1091/mbc.E08-07-0712
- Kirchhausen, T., J.S. Bonifacino, and H. Riezman. 1997. Linking cargo to vesicle formation: receptor tail interactions with coat proteins. *Curr. Opin. Cell Biol.* 9:488–495. doi:10.1016/S0955-0674(97)80024-5
- Krimbou, L., M. Tremblay, J. Davignon, and J.S. Cohn. 1998. Association of apolipoprotein E with alpha2-macroglobulin in human plasma. *J. Lipid Res.* 39:2373–2386.
- Lakadamyali, M., M.J. Rust, and X. Zhuang. 2006. Ligands for clathrin-mediated endocytosis are differentially sorted into distinct populations of early endosomes. *Cell.* 124:997–1009. doi:10.1016/j.cell.2005.12.038
- Loerke, D., M. Mettlen, D. Yarar, K. Jaqaman, H. Jaqaman, G. Danuser, and S.L. Schmid. 2009. Cargo and dynamin regulate clathrin-coated pit maturation. *PLoS Biol.* 7:e57. doi:10.1371/journal.pbio.1000057
- Maurer, M.E., and J.A. Cooper. 2006. The adaptor protein Dab2 sorts LDL receptors into coated pits independently of AP-2 and ARH. *J. Cell Sci.* 119:4235–4246. doi:10.1242/jcs.03217
- Merrifield, C.J., D. Perrais, and D. Zenisek. 2005. Coupling between clathrin-coated-pit invagination, cortactin recruitment, and membrane scission observed in live cells. *Cell.* 121:593–606. doi:10.1016/j.cell.2005.03.015
- Mettlen, M., M. Stoeber, D. Loerke, C.N. Antonescu, G. Danuser, and S.L. Schmid. 2009. Endocytic accessory proteins are functionally distinguished by their differential effects on the maturation of clathrin-coated pits. *Mol. Biol. Cell.* 20:3251–3260. doi:10.1091/mbc.E09-03-0256
- Miller, K., M. Shipman, I.S. Trowbridge, and C.R. Hopkins. 1991. Transferrin receptors promote the formation of clathrin lattices. *Cell.* 65:621–632. doi:10.1016/0092-8674(91)90094-F
- Mishra, S.K., P.A. Keyel, M.J. Hawryluk, N.R. Agostinelli, S.C. Watkins, and L.M. Traub. 2002a. Disabled-2 exhibits the properties of a cargo-selective endocytic clathrin adaptor. *EMBO J.* 21:4915–4926. doi:10.1093/emboj/cdf487
- Mishra, S.K., S.C. Watkins, and L.M. Traub. 2002b. The autosomal recessive hypercholesterolemia (ARH) protein interfaces directly with the clathrin-coat machinery. *Proc. Natl. Acad. Sci. USA.* 99:16099–16104. doi:10.1073/pnas.252630799
- Mishra, S.K., P.A. Keyel, M.A. Edeling, A.L. Dupin, D.J. Owen, and L.M. Traub. 2005. Functional dissection of an AP-2 beta2 appendage-binding sequence within the autosomal recessive hypercholesterolemia protein. *J. Biol. Chem.* 280:19270–19280. doi:10.1074/jbc.M501029200
- Morris, S.M., and J.A. Cooper. 2001. Disabled-2 colocalizes with the LDLR in clathrin-coated pits and interacts with AP-2. *Traffic.* 2:111–123. doi:10.1034/j.1600-0854.2001.020206.x
- Motley, A., N.A. Bright, M.N. Seaman, and M.S. Robinson. 2003. Clathrin-mediated endocytosis in AP-2-depleted cells. *J. Cell Biol.* 162:909–918. doi:10.1083/jcb.200305145
- Pilecka, I., M. Banach-Orlowska, and M. Miaczynska. 2007. Nuclear functions of endocytic proteins. *Eur. J. Cell Biol.* 86:533–547. doi:10.1016/j.ejcb.2007.04.004
- Putthaveedu, M.A., and M. von Zastrow. 2006. Cargo regulates clathrin-coated pit dynamics. *Cell.* 127:113–124. doi:10.1016/j.cell.2006.08.035
- Rappoport, J.Z., A. Benmerah, and S.M. Simon. 2005. Analysis of the AP-2 adaptor complex and cargo during clathrin-mediated endocytosis. *Traffic.* 6:539–547. doi:10.1111/j.1600-0854.2005.00280.x
- Saffarian, S., and T. Kirchhausen. 2008. Differential evanescence nanometry: live-cell fluorescence measurements with 10-nm axial resolution on the plasma membrane. *Biophys. J.* 94:2333–2342. doi:10.1529/biophysj.107.117234
- Stewart, M. 2007. Molecular mechanism of the nuclear protein import cycle. *Nat. Rev. Mol. Cell Biol.* 8:195–208. doi:10.1038/nrm2114
- Thomson, D.J., and A.D. Chave. 1991. Jackknife error estimates for spectra, coherences, and transfer functions. In *Advances in Spectrum Analysis and Array Processing*. S. Haykin, editor. Prentice Hall, Engelwood Cliffs, NJ. 58–113.
- Trowbridge, I.S., J.F. Collawn, and C.R. Hopkins. 1993. Signal-dependent membrane protein trafficking in the endocytic pathway. *Annu. Rev. Cell Biol.* 9:129–161. doi:10.1146/annurev.cb.09.110193.001021
- Warren, R.A., F.A. Green, and C.A. Enns. 1997. Saturation of the endocytic pathway for the transferrin receptor does not affect the endocytosis of the epidermal growth factor receptor. *J. Biol. Chem.* 272:2116–2121. doi:10.1074/jbc.272.4.2116
- Warren, R.A., F.A. Green, P.E. Stenberg, and C.A. Enns. 1998. Distinct saturable pathways for the endocytosis of different tyrosine motifs. *J. Biol. Chem.* 273:17056–17063. doi:10.1074/jbc.273.27.17056
- Wilson, B.S., J.R. Pfeiffer, M.A. Raymond-Stintz, D. Lidke, N. Andrews, J. Zhang, W. Yin, S. Steinberg, and J.M. Oliver. 2007. Exploring membrane domains using native membrane sheets and transmission electron microscopy. *Methods Mol. Biol.* 398:245–261. doi:10.1007/978-1-59745-513-8_17
- Xu, X.X., W. Yang, S. Jackowski, and C.O. Rock. 1995. Cloning of a novel phosphoprotein regulated by colony-stimulating factor 1 shares a domain with the *Drosophila* disabled gene product. *J. Biol. Chem.* 270:14184–14191. doi:10.1074/jbc.270.23.14184
- Yarar, D., C.M. Waterman-Storer, and S.L. Schmid. 2005. A dynamic actin cytoskeleton functions at multiple stages of clathrin-mediated endocytosis. *Mol. Biol. Cell.* 16:964–975. doi:10.1091/mbc.E04-09-0774